Theoretical Studies of the Spectroscopic Properties of $[Pt(trpy)C{\equiv}CR]^+$ (trpy = 2,2′,6′,2″-Terpyridine; R = H, CH_2OH, and C_6H_5)

Xin Zhou, Hong-Xing Zhang,* Qing-Jiang Pan, Bao-Hui Xia, and Au-chin Tang

State Key Laboratory of Theoretical and Computational Chemistry, Institute of Theoretical Chemistry, Jilin University, Changchun 130023, People's Republic of China

Received: January 19, 2005; In Final Form: August 6, 2005

Electronic structures and spectroscopic properties of $[Pt(trpy)C{\equiv}CR]^+$ (trpy = 2,2′, 6′,2″-terpyridine; R = H (**1**), CH_2OH (**2**), and C_6H_5 (**3**)) are studied by ab initio and DFT methods. The ground- and excited-state structures are optimized by the MP2 and CIS methods, respectively. The absorption and emission spectra in the dichloromethane solution are obtained by using TD-DFT (B3LYP) method associated with the PCM model. The calculations indicate that, for **1**−**3**, the variation of the substituents on the acetylide ligand only slightly changes their structures in ground and excited states but leads to a sizable difference in the electronic structures. In both cases of absorption and emission, the energy levels of HOMOs for **1**−**3** are sensitive to the substituents on acetylide ligand and increase obviously with the introduction of the electron-donating groups; however, those of trpy-based LUMOs vary slightly. The lowest-energy emissions are attributed to triplet acetylide/Pt → trpy charge transfer (^{3}LLCT/^{3}MLCT) transitions and the lowest-energy absorptions and emissions for **1**−**3** are red-shifted on the order of **1** < **2** < **3** when the electron-donating groups are introduced into the acetylide ligand. By comparison of the results obtained by using different functionals in TD-DFT method, the calculations indicate that the exchange-correlation functionals (B3LYP, B3P86 and B3PW91) involving Becke three parameter hybrid functionals are appropriate for the terpyridyl platinum(II) acetylide complexes to get the relatively satisfactory results for the absorption spectra. The underestimated excitation energies of lowest-lying absorption bands are probably due to insufficient flexibility in TD-DFT method to describe states with large charge transfer.

I. Introduction

Platinum(II) complexes have been extensively investigated by experiments[1] over the past few decades, due to their rich spectroscopic properties. A wide range of Pt(II) complexes have been synthesized and structurally characterized, and the corresponding absorptions and emissions have also been explored in considerable details.[2] The emission spectra displayed a variety of electronic excited states responsible for the phosphorescence of the complexes: ^{3}MC (metal centered), ^{3}MLCT (metal-to-ligand charge transfer), ^{3}LLCT (ligand-to-ligand charge transfer), $^3\pi \rightarrow \pi^*$, and ^{3}MMLCT (metal-to-metal-to-ligand charge transfer) transitions.[3]

Recently, people's interests were focused on the terpyridyl Pt(II) complexes and their derivatives such as $[Pt(trpy)R]^+$ and $[Pt(4\text{-}X{-}T)R]^+$ (X = ph, Ar, Me, C_6H_4Me and tolyl; R = Cl, CN, NCS, OH, OMe, and MeCN) because of their unique spectroscopic properties and intense luminescence in solid and solution in visible region. Yam et al. and Yang et al. found that the terpyridyl Pt(II) acetylide complexes[4] can exhibit long-lived emissions and large quantum yields with respect to other complexes, and tentatively assigned the lowest-energy emissions as the phosphorescence arising from the ^{3}MLCT/^{3}LLCT transition. In general, the nature of the spectra is related to the character of the substituted ligands. The efficient radiationless decay via a low-lying ^{3}d−d state has been suggested as the intrinsic reason for no detectable emission in fluid solution for the $[Pt(trpy)Cl]^+$ complexes.[5] However, the introduction of substituents such as aryl groups into the terpyridyl ligand results in the Pt(II) complexes highly emitting in solution,[6] because the delocalization of the aryl groups stabilizes the LUMOs (lowest unoccupied molecular orbitals) and increases the energy gap between the charge transfer and d−d transition. Furthermore, if the Cl anion of $[Pt(trpy)Cl]^+$ is replaced with a rich-electron ligand such as NCS, CH_3, OCH_3, and phenyl et al.,[5,7] the ^{3}MLCT, ^{3}LLCT, and $^3\pi \rightarrow \pi^*$ transitions can be expected.

Absorption and emission spectra of the terpyridyl Pt(II) complexes are usually sensitive to the environment. For example, Yip et al. have reported the phosphorescence of the $[Pt(trpy)Cl]CF_3SO_3$ salt at room temperature as well as 77K in the solid,[8] but no emission has been found for $[Pt(trpy)Cl]^+$ in solution at room temperature. Moreover, the difference in electronic structure also plays an important role in the absorption and emission. The emission of $[Pt(trpy)(MeCN)](SbF_6)$ in solid state at room-temperature was attributed to a $\pi\pi^*$ character,[9] but that of $[Pt(trpy)R]^+$ (R═Cl and C≡Ph et al.) was regarded as a MMLCT character.[4a,10]

On the basis of the experimental results, the terpyridyl Pt(II) acetylide complexes can be a kind of promising luminescent material with a variety of electronic excited states. To provide the experimental results a powerful theoretical support£×c2we calculate three complexes, $[Pt(trpy)C{\equiv}CR]^+$ (trpy = 2,2′, 6′,2″-terpyridine; R═H (**1**), CH_2OH (**2**) and C_6H_5 (**3**)), and reveal the substituent effects upon electronic structures and spectroscopic properties. The calculation indicates that the ^{3}LLCT/^{3}MLCT transition is responsible for the lowest-energy phosphorescence for **1**−**3**. The phosphorescent emissions are red-shifted

* To whom correspondence should be addressed. E-mail: hxzhang@mail.jlu.edu.cn.

10.1021/jp0503359 CCC: $30.25
Published on Web 09/09/2005

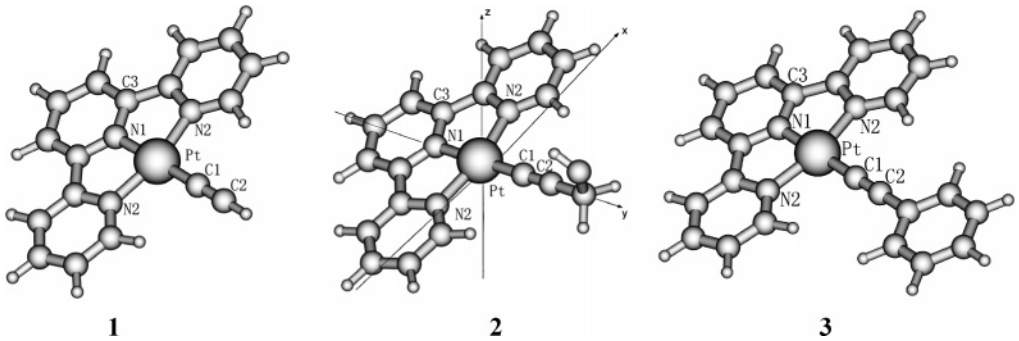

Figure 1. Optimized ground-state structures for $[Pt(trpy)C{\equiv}CH]^+$ (**1**), $[Pt(trpy)C{\equiv}CCH_2OH]^+$ (**2**), and $[Pt(trpy)C{\equiv}CC_6H_5]^+$ (**3**) under MP2 methods, respectively.

in the order **1** < **2** < **3** as the ability of electron-donating of substituents increases.

II. Computational Details and Theory

The second-order Møller−Plesset perturbation (MP2)[11] and single-excitation configuration interaction (CIS) methods[12] are employed to optimize the ground and excited-state structures for **1**−**3**, respectively. The MP2 calculations reveal that the ground-states are $^1A_1$, $^1A'$, and $^1A_1$ for **1**, **2**, and **3** with the $[36(a_1^2)27(b_2^2)8(b_1^2)5(a_2^2)]$, $[50(a'^2)34(a''^2)]$, and $[46(a_1^2)34(b_2^2)10(b_1^2)6(a_2^2)]$ electronic configurations, respectively. On the basis of the optimized structures in ground and excited states, the spectroscopic properties related to absorption and emission in dichloromethane are obtained by the time-dependent density functional theory (TD-DFT)[13] at B3LYP functional (Becke's three parameter functional and the Lee−Yang−Parr functional)[14] associated with the polarized continuum model (PCM).[15]

The optimized ground-state structures for **1**−**3** are illustrated in Figure 1 together with the molecular coordinate orientation. In the calculations, the terpyridyl ligand lies on the *xy* plane and the *z* axis is perpendicular to the plane of terpyridyl ligand; Pt(II) atom and acetylide ligand orient the *y* axis.

For **1**−**3**, the coordination geometry of Pt(II) keeps the quasi square planar conformation, as illustrated in Figure 1. In the calculations, C_{2v} symmetry is adopted to **1** and **3**, while C_s symmetry is adopted to **2**, since the CH_2OH substituent breaks the C_{2v} symmetry. With respect to **3**, the plane of phenyl group is placed parallel to the terpyridyl plane, because the extended π-conjugation among the whole complex stabilizes the conformation. The X-ray diffraction of $[Pt(trpy)C{\equiv}CC_6H_5]^+$ have proved that the phenyl ring on the acetylide ligand is only twisted by a angle of 5.6° to the plane of Pt(II)−terpyridine.[5a]

It is well-known that, for excited states, the CIS method is most similar for the HF method to the ground state. However through the using of analytic gradients and methods properly including the effects of electronic correlation, the bond lengths, frequencies, and dipole moments at the CIS level are well in line with the experimental values as well as the application of the method to very large molecules is possible.[12] Though the reasonable excited-state structures can be obtained by CIS method, the predicted transition energies deviate from experimental values commonly about 1 eV or more. In recent years, TD-DFT methods have been successfully used to calculate singlet−singlet and singlet−triplet transitions in many reports.[16] More electronic correlations are involved in the TD-DFT (B3LYP) approach, which then yields more accurate excitation energies than CIS method. This approach overcomes many of the problems encountered in vertical energies with the CIS method, providing accurate excitation energies of valence and Rydberg states. To obtain the accurate excited-state geometry and excitation energies, on the basis of CIS optimized structures of the excited states, we employ the TD-DFT method to calculate the excitation energies in emission. Since the accurate excited-state structure by the CIS method and excitation energy by the TD-DFT method can be obtained, the combination of the two methods will be expected to predict the preferable geometry and electronic structures as well as excited-state properties in emission. In this calculation, we optimize the excited-state structures for **1**−**3** by CIS method and correct their excitation energies by using the TD-DFT approach.

TABLE 1: Optimized Main Geometry Parameters of the Ground State and the Triplet Excited State for $[Pt(trpy)C{\equiv}CH]^{+-}$ (1), $[Pt(trpy)C{\equiv}CCH_2OH]^+$, (2) and $[Pt(trpy)C{\equiv}CC_6H_5]^+$ (3) Using the MP2 and CIS Methods, Respectively, Together with the Experimental Values

	1		**2**		**3**		
state	$^1A_1$	$^3A_1$	$^1A'$	$^3A'$	$^1A_1$	$^3A_1$	expt[a]
			Bond Length [Å]				
Pt−N(1)	2.005	1.997	2.016	2.001	2.002	1.996	1.97
Pt−N(2)	2.040	2.070	2.050	2.074	2.037	2.071	2.02
Pt−C(1)	1.970	2.003	1.973	2.008	1.966	2.000	1.98
N(1)−C(3)	1.377	1.361	1.376	1.361	1.378	1.361	1.34
C(1)−C(2)	1.255	1.213	1.257	1.213	1.261	1.216	1.19
			Bond Angle [deg]				
N(1)−Pt−N(2)	81.1	80.5	80.9	80.4	81.2	80.3	80.8

[a] From ref 5a.

In the calculation, quasirelativistic pseudopotential of the Pt(II) atom proposed by Hay and Wadt[17] with 18 valence electrons is employed, and the LANL2DZ basis sets associated with the pseudopotential are adopted. To precisely describe the molecular properties, one additional f-type polarization function is implemented for Pt(II) atom ($\alpha = 0.14$).[18] The basis sets (8s6p3d1f/3s3p2d1f) for the Pt(II) atom and (10s5p/3s2p), (10s5p/3s2p), and (4s/2s) for N, C, and H are used for the valence shell, respectively. Therefore, 233 basis functions and 152 electrons for **1**, 255 basis functions and 168 electrons for **2**, and 295 basis functions and 192 electrons for **3** are included in the calculations. All the calculations are accomplished by using the Gaussian03 (Revision B.03) program package on an Origin/3900 server.[19]

III. Results and Discussions

III.A. The Ground-State Structures and the Absorption Spectra in the CH_2Cl_2 Solution. The ground-state structures for **1**−**3** are fully optimized by the MP2 method. The optimized structures are illustrated in Figure 1 and corresponding main geometrical parameters are listed in Table 1. The bond angles of N(1)−Pt−N(2) are about 81° for **1**−**3**, corresponding well

TABLE 2: Absorptions of $[Pt(trpy)C{\equiv}CH]^{+-}$ (1), $[Pt(trpy)C{\equiv}CCH_2OH]^+$ (2), and $[Pt(trpy)C{\equiv}CC_6H_5]^+$ (3) in Dichloromethane under TD-DFT (B3LYP) Calculations, Together with Experimental Values

	transition	config (CI coeff)	*E*, nm (eV)	oscillator	assignment
1	$X^1A_1 \rightarrow A^1A_1$	$8b_1 \rightarrow 9b_1$ (0.68)	465 (2.67)	0.069	LLCT/MLCT
	$X^1A_1 \rightarrow B^1B_1$	$36a_1 \rightarrow 9b_1$ (0.70)	433 (2.87)	0.0031	MLCT
	$X^1A_1 \rightarrow C^1B_2$	$8b_1 \rightarrow 6a_2$ (0.70)	411 (3.02)	0.021	LLCT/MLCT
	$X^1A_1 \rightarrow D^1B_2$	$4a_2 \rightarrow 9b_1$ (0.66)	330 (3.76)	0.36	$\pi \rightarrow \pi^*$/MLCT
2	$X^1A' \rightarrow A^1A'$	$50a' \rightarrow 51a'$ (0.67)	527 (2.35)	0.081	LLCT/MLCT
	$X^1A' \rightarrow B^1A''$	$50a' \rightarrow 35a''$ (0.70)	473 (2.62)	0.017	LLCT/MLCT
	$X^1A' \rightarrow C^1A'$	$49a' \rightarrow 51a'$ (0.70)	427 (2.91)	0.0020	MLCT
	$X^1A' \rightarrow D^1A''$	$31a'' \rightarrow 51a'$ (0.64)	327 (3.80)	0.22	$\pi \rightarrow \pi^*$/MLCT
3	$X^1A_1 \rightarrow A^1A_1$	$10b_1 \rightarrow 11b_1$ (0.68)	586 (2.12)	0.19	LLCT/MLCT
	$X^1A_1 \rightarrow B^1B_2$	$10b_1 \rightarrow 7a_2$ (0.70)	498 (2.50)	0.019	LLCT/MLCT
	$X^1A_1 \rightarrow C^1B_1$	$46a_1 \rightarrow 11b_1$ (0.70)	432 (2.88)	0.0029	MLCT
	$X^1A_1 \rightarrow D^1B_2$	$4a_2 \rightarrow 11b_1$ (0.66)	332 (3.74)	0.30	$\pi \rightarrow \pi^*$/MLCT

[a] From ref 5a. [b] From ref 5b.

TABLE 3: Partial Molecular Orbital Compositions in the Ground State for $[Pt(trpy)C{\equiv}CH]^+$ (1) in Dichloromethane under the TD-DFT Calculations

			contribution (%)			Pt components (%)	
orbital	energy (eV)	bond type	Pt	trpy	C≡C		
$11b_1$	−1.1442	d(Pt) + π^*(trpy)	38.2	52.2	9.5		30.0 $d_{x^2-y^2}$
$37a_1$	−1.3796	π^*(trpy)		99.3			
$7a_2$	−2.1100	π^*(trpy)		97.1			
$10b_1$	−2.1552	π^*(trpy)		99.6			
$6a_2$	−3.0801	π^*(trpy)		98.0			
$9b_1$	−3.4953	π^*(trpy)		93.2			
		HOMO−LUMO Energy Gap					
$8b_1$	−6.7447	d(Pt) + π(C≡C)	42.6	10.4	46.8		42.4 d_{yz}
$27b_2$	−6.9830	d(Pt) + π(C≡C)	27.4	18.2	54.2		25.9 d_{xy}
$36a_1$	−7.3066	d(Pt)	94.9			14.3 s	80.6 d_{z^2}
$5a_2$	−7.4056	d(Pt) + π(trpy)	54.8	45.2			54.8 d_{xz}
$4a_2$	−7.8465	d(Pt) + π(trpy)	22.1	77.9			22.1 d_{xz}

to the experimental values of 80.8°,[5a] indicating that the coordination geometry of Pt(II) exhibits nearly square planar conformation. The geometries of terpyridyl Pt(II) for **1**−**3** are quite insensitive to the R groups (H, CH_2OH, and C_6H_5) on acetylide ligand, just as observed in the experiments**.** For **1**−**3**, the calculated Pt−N(1) and Pt−N(2) bond lengths range from 2.00 to 2.05 Å corresponding to the experimental values from 1.97 to 2.02 Å, respectively.[5a] The distance of N(1)−C(3) for **1**−**3** is ca. 1.36 Å and is much shorter than a normal C−N single bond length of 1.48 Å, indicating that there are some delocalization of the lone pairs of the central amine nitrogens into the pyridine rings. On the basis of the optimized ground-state structures mentioned above, the electronic structures related to absorptions are carried out by using the TD-DFT method, and the PCM model is combined to reveal the spectroscopic properties for **1**−**3** in solution. In the calculations, the single molecular model is adopted to simulate the spectroscopic properties in dilute solution. It has been proved that the absorptions of the $[Pt(trpy)C{\equiv}CR]^+$ complexes obey Beer's law in the concentration range of 10^{-5}−10^{-2} mol dm^{-3} in dimethylformamide.[5a] It indicates that there is a little aggregation for the complexes in solution. The calculated absorptions associated with their excitation energies and oscillator strengths as well as the assignments of the transitions are available in Table 2.

To clearly discuss the absorption spectra in solution, the partial frontier orbitals compositions of **1** are listed in Table 3. With respect to **1**, as seen in Table 3, occupied MOs are almost filled with substantial metal Pt(II) atom and virtual MOs are localized on the terpyridyl ligand mainly. Four low-lying dipole-allowed absorptions calculated at 465, 433, 411, and 330 nm are attributed to the LLCT/MLCT, MLCT, LLCT/MLCT, and $\pi \rightarrow \pi^*$/MLCT transitions, respectively.

With respect to the 465 nm lowest-energy absorption, the $8b_1 \rightarrow 9b_1$ excitation corresponds to the largest CI coefficient of 0.68. As seen in Table 3, $8b_1$ MO is the highest occupied MO (HOMO, π^*(Pt−C≡C)) composed of about 43% metal Pt(II) and 47% acetylide ligand, while the $9b_1$ MO, the LUMO, lying above the HOMO by about 3.25 eV, is mainly localized on the terpyridyl ligand with the 93% composition. Therefore, the lowest-energy absorption with oscillator strength of 0.0694 arising from the $X^1A_1 \rightarrow A^1A_1$ transition is assigned as the C≡C + Pt(II) → trpy charge transfer (LLCT/MLCT). For the 433 nm absorption from the $X^1A_1 \rightarrow B^1B_1$ transition, the $36a_1 \rightarrow 9b_1$ excitation corresponding to the largest CI coefficient of 0.70 dominates the absorption. As indicated in Table 3, $36a_1$ MO, ∼0.55 eV lower than $8b_1$(HOMO), is pure metal-based involving substantial Pt(II) d_{z^2} (81%) and some 6s atomic orbital (14%). Thus, the absorption at 433 nm is attributed to the Pt-(II) atom ($5d_{z^2}$ + 6s) → π^* (trpy) charge transfer (pure-MLCT) transition. With regard to the C^1B_2 excited state, the 411 nm absorption is mainly contributed from $8b_1 \rightarrow 6a_2$ excitation (CI coefficient = 0.70). As presented in above sections, the most virtual MOs are essentially trpy-based. From Table 3, the $6a_2$ MO (LUMO+1) is located on the terpyridyl ligand 98%. We can attribute the lower-lying absorption at 411 nm to the LLCT/MLCT character which is similar to the lowest-energy absorption in nature. In the four low-lying absorptions, the 330 nm absorption with the largest oscillator strength of 0.36 is expected as one of the most easily observed absorption in experiments. In the $X^1A_1 \rightarrow D^1B_2$ transition, two excitations contribute to the transition. One is $4a_2 \rightarrow 9b_1$ excitation corresponding to the CI coefficient of 0.66, the other is $5a_2 \rightarrow 10b_1$ excitation corresponding to the CI coefficient of 0.15. Owing to the large difference of CI coefficient between them, the assignment of the highest-energy absorption should correspond to the $4a_2 \rightarrow 9b_1$

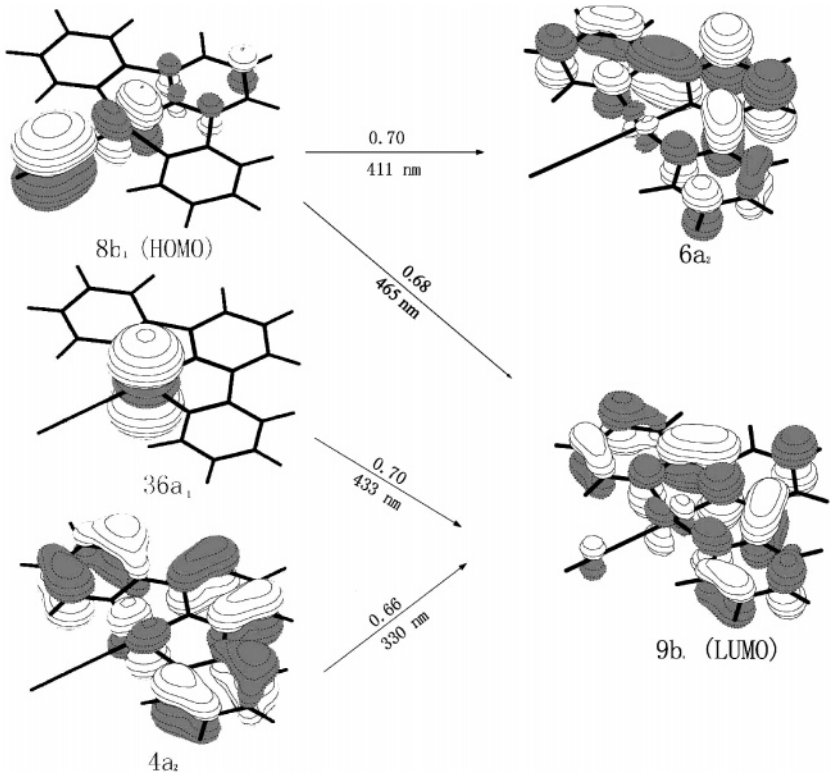

Figure 2. Single electron transitions with the maximum CI coefficients under TD-DFT calculations for the 433, 411, and 330 nm absorptions of $[Pt(trpy)C{\equiv}CH]^+$ (**1**) in dichloromethane.

TABLE 4: Partial Molecular Orbital Compositions in the Ground State for $[Pt(trpy)C{\equiv}CCH_2OH]^+$ (2) in Dichloromethane under the TD-DFT Calculations

			contribution (%)				Pt components (%)	
orbital	energy (eV)	bond type	Pt	trpy	C≡C	CH_2OH		
54a′	−2.1394	d(Pt) + π*(trpy)	37.9	54.6	7.2			31.4 $d_{x^2-y^2}$
53a′	−2.4202	π*(trpy)		99.3				
36a″	−3.1078	π*(trpy)		97.1				
52a′	−3.1576	π*(trpy)		99.6				
35a″	−4.1332	π*(trpy)		98.1				
51a′	−4.4935	π*(trpy)		92.3				
		HOMO−LUMO Energy Gap						
34a″	−7.2492	d(Pt) + π(C≡C) + $\sigma(CH_2OH)$	15.8	12.3	41.8	30.0		14.5 d_{xy}
50a′	−7.3425	d(Pt) + π(C≡C) + $\sigma(CH_2OH)$	29.8	8.0	52.1	10.0		29.2 d_{yz}
33a″	−7.9746	π(C≡C) + $\sigma(CH_2OH)$	6.6	4.8	16.0	72.6		6.1 d_{xy}
49a′	−8.3469	d(Pt)	94.7				12.4 s	82.3 d_{z^2}
32a″	−8.4097	d(Pt) + π(trpy)	59.5	40.5				59.5 d_{zz}
31a″	−8.8691	d(Pt) + π(trpy)	17.4	82.6				17.4 $_{xz}$

excitation. As depicted in Table 3, the $4a_2$ MO is localized on terpyridyl ligand (ca. 78%) perturbed by some metal Pt(II) contribution (ca. 22%), so the 330 nm absorption is assigned to the $\pi \rightarrow \pi^*$ transition within the terpyridyl ligand and mixed with some MLCT characters. To intuitively understand the absorption of **1** in solution, we display the electron density diagrams in Figure 2, in which four single electron excitations corresponding to the maximal CI coefficients are involved. With respect to the 433 nm absorptions, the electron density diagram shows that the charges transfer from Pt(II) atom to π*-bonding located on the terpyridyl ligand, which are in accordance to the MLCT transition.

In the virtual MOs, as listed in Table 3, $11b_1$ MO, lying above $9b_1$ MO (LUMO) about 2.35 eV, features ca. 30% Pt(II) $d_{x^2-y^2}$ atomic orbital. As mentioned above, $36a_1$ MO is a pure metal-based orbital (d_{z^2} + s). Therefore, the separated d−d transition energy is about 6.1 eV, far larger than that of charge transfer, indicating that the d−d transition does not easily occur in absorption. Moreover, the introduction of the substituted acetylide group succeeds in separating the energy gap between d−d and charge-transfer transitions.

It is analogous to **1**, to analyze the absorption spectra of **2** and **3**, we list their corresponding compositions of frontier orbitals in Tables 4 and 5. As seen in the tables, unoccupied MOs are dominated by π antibonding located upon the terpyridyl ligand, while occupied MOs are localized on the Pt(II) atom, acetylide ligand and its substituents. The introduction of electron-donating substituents into the acetylide ligand results in the relevant change of the compositions of occupied frontier orbitals for **2** and **3**.

With respect to **2** and **3**, the two lowest-lying absorptions are calculated at 527 and 473 nm for **2** and 586 and 498 nm for **3**, respectively. From the tables, the 50a′ MO (HOMO-1) of **2** involves 30% Pt(II), 52% C≡C, and 10% CH_2OH group, while the $10b_1$ MO (HOMO) of **3** results from 20% Pt(II), 36% C≡C, and 38% C_6H_5, respectively. The LUMO and LUMO+1 of **2** and **3** are a set of quasi degenerate orbitals and localized on the terpyridine above 90%. Thus, the two lowest-lying

TABLE 5: Partial Molecular Orbital Compositions in the Ground State for $[Pt(trpy)C{\equiv}CC_6H_5]^+$ (3) in Dichloromethane under the TD-DFT Calculations

			contribution (%)				Pt components (%)	
orbital	energy (eV)	bond type	Pt	trpy	C≡C	C_6H_5		
$47a_1$	−1.1287	d(Pt) + π*(trpy)	38.4	54.2	6.7			31.2 $d_{x^2-y^2}$
$14b_1$	−1.1581	π*(−C_6H_5)	6.7	7.2	12.1	73.9		
$13b_1$	−1.3840	π*(trpy)		97.5				
$8a_2$	−2.1149	π*(trpy)		97.1				
$12b_1$	−2.1617	π*(trpy)		99.6				
$7a_2$	−3.0812	π*(trpy)		98.0				
$11b_1$	−3.5051	π*(trpy)		91.6				
		HOMO−LUMO Energy Gap						
$10b_1$	−6.0913	d(Pt) + π(C≡C) + π(C_6H_5)	19.9	6.3	35.7	38.1		19.3 d_{yz}
$34b_2$	−6.9039	d(Pt) + π(C≡C) + π(C_6H_5)	23.7	16.2	49.2	10.6		22.5 d_{xy}
$6a_2$	−7.1898	π(C_6H_5)				100.0		
$46a_1$	−7.3243	d(Pt)	94.8				14.3 s	80.5 d_{z^2}
$5a_2$	−7.4097	d(Pt) + π(trpy)	53.7	46.3				53.7 d_{xz}
$9b_1$	−7.7882	d(Pt) + π(trpy) + π(C_6H_5)	40.8	16.7		37.1		40.8 d_{yz}
$4a_2$	−7.8514	d(Pt) + π(trpy)	23.2	76.8				23.2 d_{xz}

absorptions for **2** and **3** are all assigned to ligand (C≡CR) → ligand (trpy) charge transfer (LLCT) mixed some metal (Pt) → ligand (trpy) charge transfer (MLCT). For the lowest-energy 586 nm absorption of **3**, the oscillator strength of 0.19 is far larger than that of corresponding lowest-energy absorption of **1** and **2**. The phenomenon can be attributed to the presence of the strong resonance forms when strong electron-donating phenyl group are attached at the acetylide ligand.

For the C^1A' and C^1B_1 excited states of **2** and **3**, the 49a′ and $46a_1$ MOs are metal-based orbitals and contributed by significant Pt(II) d_{z^2} atomic orbital about 95%. Associated with the electronic density diagrams depicted in Figures S1 and S2, the 427 and 432 nm absorptions with small oscillator strength, originating from the $X^1A'\rightarrow C^1A'$ and $X^1A_1\rightarrow C^1B_1$ transitions, respectively, are assigned to the metal (d_{Pt}) → ligand (trpy) charge transfer (MLCT) transition like that in **1**. Additionally, because the $X^1A' \rightarrow D^1A''$ and $X^1A_1 \rightarrow D^1B_2$ transitions for **2** and **3** are mainly occurring on the terpyridyl ligand, the 327 and 332 nm absorptions with the largest oscillator strength of about 0.2 and 0.3 for **2** and **3**, respectively, are due to the characterized $\pi \rightarrow \pi^*$ transition, being analogous to the high-lying absorptions of **1** which we have discussed above.

With reference to the previous experimental assignments,[4] the absorption bands at 300−350 nm probably arise from the intraligand (IL) transition of the trpy ligands as well as the charge-transfer transition involved in the Pt−C≡CR moieties, while the absorption bands at ca. 420−430 nm are assigned as the MLCT transition. Additionally, both of the absorption bands are insensitive to the variation of the substituted acetylide ligands. As mentioned above, our calculated excitation energies and assignments of the last two absorption bands are well consistent with the experimental description. However, there is a slight difference in the excitation energy of lowest-energy absorption bands. Recently, Guo et al. investigated a series of platinum terpyridyl acetylide complexes and found a low-lying charge-transfer band at 460−540 nm with weak intensity, which is sensitive to the substituted acetylide ligands and is assigned to the Pt/acetylide → trpy charge-transfer transition. In our calculation, we obtain the lowest-energy absorptions at 465−580 nm for **1**−**3** that are sensitive to the substituted acetylide ligand and should be responsible for the experimental observed. The calculated maxima of lowest-energy absorption bands are red-shifted compared to those in experiment; this is probably due to insufficient flexibility in the TD-DFT method to describe states with large charge transfer.[20] To check whether the B3LYP functional is appropriate to our calculations, we again calculate the absorption spectra by using different functionals in the TD-DFT method. The calculated transitions together with excitation energies and oscillator strengths are listed in Table S1 (see Supporting Information). As seen in Table S1, the discrepancies of the excitation energies calculated by B3LYP, B3P86, and B3PW91 are less than 0.03 eV and by BP86 and BPW91 as well as SVWN less than 0.04 eV, respectively. However, the excitation energies of the first two absorption bands for **1**−**3** are higher about 0.5−0.7 eV by hybrid functionals, i.e., B3LYP, B3P86, and B3PW91, than by BP86 and BPW91 as well as SVWN functionals. On the basis of the experimental values, the excitation energies related to absorption computed by BP86, BPW91, and SVWN functionals even lower than the corresponding phosphorescent emissive energies. Since the emissive energy must be lower than the absorption energy, it is obvious that the three functionals are not appropriate to describe the behaviors of the absorption transitions with large charge transfer. The calculated third absorption band with MLCT character again proves above viewpoint. The computed excitation energies at BP86, BPW91, and SVWN functionals level are about 0.5−0.7 eV lower than those in B3LYP, B3P86, and B3PW91 functionals, but the values calculated by B3LYP, B3P86, and B3PW91 functionals are well in accordance with the experiments. That is to say that the results obtained by B3LYP, B3P86, and B3PW91 functionals are correspondingly reliable. In our calculation, although the excitation energies related to the lowest-lying absorption bands are higher than the corresponding experimental values, overall, the experimental spectra are well reproduced by the B3LYP functional, in particular for the absorptions with the $\pi \rightarrow \pi^*$ and MLCT characters. It has been suggested that the excitation energy in absorption spectra is sensitive to the selection of functional. The calculations indicate that the exchange-correlation functionals (B3LYP, B3P86, and B3PW91) involving Becke three parameter hybrid functionals are appropriate for the terpyridyl Pt(II) acetylide complexes to get the relatively satisfactory results for the absorption spectra.

III.B. Substituent Effects on Absorption Spectra. To probe the nature of the substituent effects on absorption spectra, on the basis of the calculated each excited states with $f > 0$, we simulate the absorption spectra for **1**−**3** with Gaussian curves. The fit absorption curves are depicted in wavelength vs oscillator strength in Figure 3. The full width at half-maximum of each Gaussian curve is evaluated to be 10 nm based on the narrowest peak of absorption for $[Pt(4\text{-Ph-T})Cl]^+$ in DCM at room temperature.[6a] Because the narrowest peak of absorption for terpyridyl Pt(II) complexes always arises from the $\pi \rightarrow \pi^*$

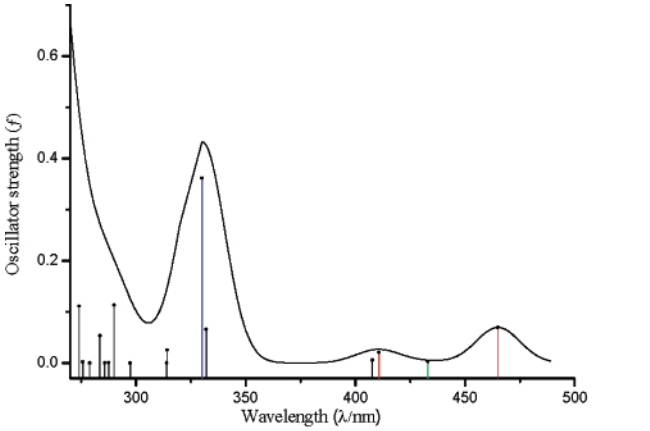

1

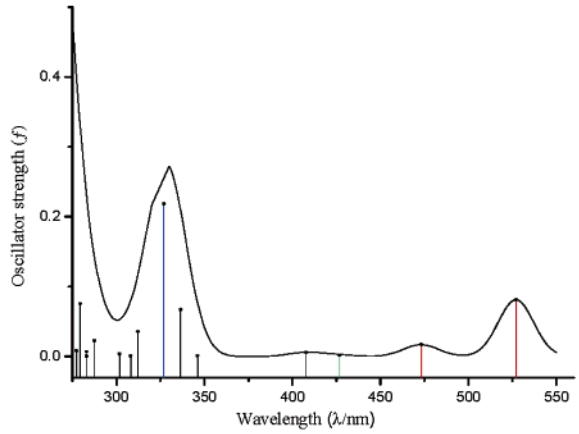

2

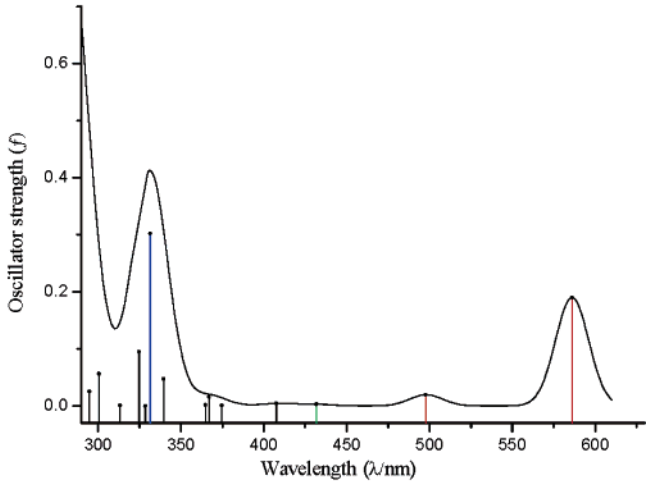

3

Figure 3. Simulated absorption spectra with Gaussian curve based on the data calculated under the TD-DFT method in dichloromethane for **1**−**3**. (Excited states listed in Table 2 are colored. Blue lines: $\pi \rightarrow \pi^*$/MLCT transition. Green line: MLCT transition. Red line: LLCT/MLCT transition.)

involved in the terpyridine, we think that the selection of the full width is appropriate for **1**−**3**.

As illustrated in Figure 3, the colored excited states correspond to the character of LLCT/MLCT (red), MLCT (blue) and $\pi \rightarrow \pi^*$/MLCT (green), respectively. The shapes of the absorption spectra keep identical by and large for **1**−**3**, except for the first two low-lying absorptions, which arise from the LLCT/MLCT transition, being red-shifted as the electron-donating ability of the substituents increase. The evidence strongly suggests that only the LLCT/LLCT transitions are sensitive to substituents on acetylide ligand, while the transitions originating from pure-MLCT and $\pi \rightarrow \pi^*$ are not affected by the substituents basically.

To further shed light on how substituents affect the electronic transitions, the orbital energy levels for **1**−**3** are illustrated in Figure 4. Through the diagrams of energy level, we can understand the above question why LLCT/MLCT transitions are sensitive to the variation of substituents. If we assume that the LUMOs have the identical orbital energy levels for **1-3**, then the replacement between CH_2OH and C_6H_5 groups and hydrogen atom raises the energy level of HOMOs. The excitation energies of lowest-lying absorptions which arise from the LLCT/MLCT transitions are 3.87 and 3.25 eV for **1**, 3.21 and 2.85 eV for **2**, and 3.01 and 2.59 eV for **3**, respectively. The regressive trend of the excitation energies on going from **1** to **3** is in accordance with the peaks of the absorptions being red-shifted as the ability of electron-donating of substituents increases. The excitation energies of pure-MLCT transitions are 3.81, 3.85, and 3.82 eV and those of $\pi \rightarrow \pi^*$ transitions are 4.35, 4.38, and 4.35 eV for **1**−**3**, respectively. They are responsible for the unchangeable trend of low-lying absorption.

In addition, we have mentioned previously that the d−d transition is the intrinsic reason for the emissionless in solution. Effectively separating the energy gap between the d−d and HOMO−LUMO through varying the substituents can offer a useful guide to synthesize the efficient luminescent materials. The energy gaps between them are increased in the order 2.9 (**1**) < 3.45 (**2**) < 3.61 (**3**) eV according to the electron-donating ability of H < CH_2OH < C_6H_5, indicating that **3** is the best candidate for luminescent materials among the three complexes.

III.C. The Lowest-Energy Excited-State Structures and Emission Spectra in the CH_2Cl_2 Solution. On the basis of the optimized ground-state structures, the lowest-energy excited-state structures of **1**−**3** are fully optimized out by the CIS method. Upon excitation for **1**−**3**, the structures still keep coplanar and bear similarity with respect to those of the ground states. The main geometry parameters have a minor change compared to those of ground states as shown in Table 1. A general elongations of bond lengths about 1.5% between Pt(II) and ligands for **1**−**3** are observed except for Pt−N(1) bond lengths, which are shortened by about 0.5%. The variation of bond lengths corresponds to the electron being promoted from the Pt(II) atom to terpyridyl and acetylide ligands and to the interaction between the Pt(II) atom and ligands being weak upon excitation. The evidence suggests that ^{3}LLCT/^{3}MLCT transition should be responsible for the lowest-energy emission. For **1**, the Pt−N(2) and Pt−C bond lengths slightly elongate ca. 0.03 Å compared with those in the ground state; instead, the Pt−N(1) bond length is shortened slightly. The analogous trends are also observed in **2** and **3**.

In view of obtaining the convincible emissive energies, based on the excited-state structures optimized by the CIS method, the emission spectra of **1**−**3** in dichloromethane are calculated by TD-DFT approach at B3LYP level associated with PCM model. The corresponding emissions for **1**−**3** are listed in Table 6 associated with the emissive energies and transition assignments.[5a] The calculated lowest-energy phosphorescence in the dichloromethane solution for **1**−**3** is at 513, 584, and 614 nm, respectively. The phosphorescent emissions are assigned to the ^{3}LLCT/^{3}MLCT characters. We have presented in my above discussions that the lower-energy absorptions calculated at 465, 527, and 586 nm also arise from the LLCT/MLCT transition. Since the lowest-energy emissions and absorptions have the

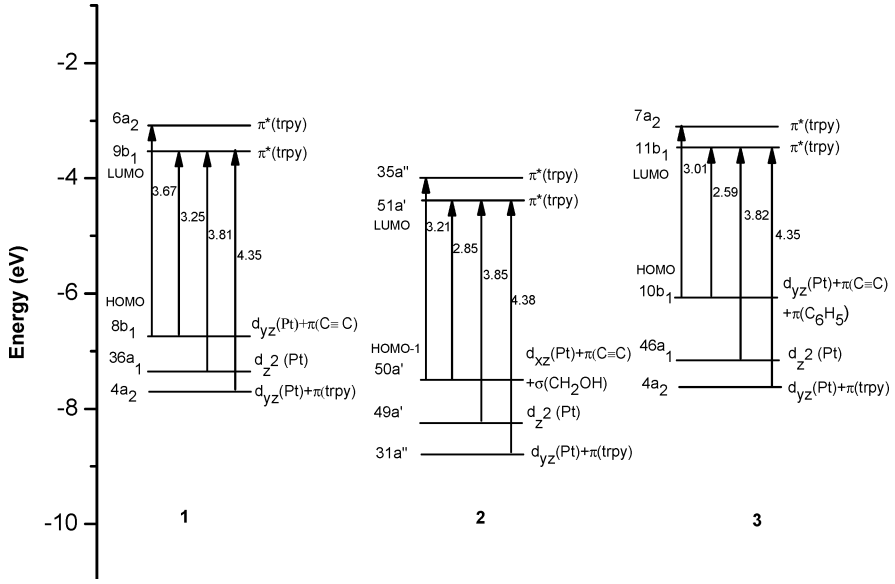

Figure 4. Diagrams of energy levels of orbitals involved in the absorptions for [Pt(trpy)C≡CH]$^+$ (**1**), [Pt(trpy)C≡CCH$_2$OH]$^+$ (**2**), and [Pt(trpy)C≡CC$_6$H$_5$]$^+$ (**3**) under TD-DFT calculations.

TABLE 6: Phosphorescent Emissions of [Pt(trpy)C≡CH]$^{+-}$ (1), [Pt(trpy)C≡CCH$_2$OH]$^+$ (2), and [Pt(trpy)C≡CC$_6$H$_5$]$^+$ (3) in Dichloromethane under the TD-DFT(B3LYP) Calculations, Together with Experimental Values

	transition	config. (CI coeff)	tran. energy in nm (eV)	transition character	λ_{em} in expt (character)
1	$^3A_1 \rightarrow {}^1A_1$	$9b_1 \rightarrow 8b_1$ (0.70)	513 (2.42)	^{3}LLCT/^{3}MLCT	
2	$^3A' \rightarrow {}^1A'$	$51a' \rightarrow 50a'$ (0.71)	584 (2.13)	^{3}LLCT/^{3}MLCT	552/(^{3}LLCT/^{3}MLCT)[b]
3	$^3A_1 \rightarrow {}^1A_1$	$11b_1 \rightarrow 10b_1$ (0.70)	614 (2.02)	^{3}LLCT/^{3}MLCT	630/(^{3}LLCT/^{3}MLCT)[a] 618/(^{3}LLCT/^{3}MLCT)[b]

[a] From ref 5a. [b] From ref 5b.

TABLE 7: Partial Molecular Orbital Contributions (%) in the Lowest-Energy $^3A_1$ Excited-States for [Pt(trpy)C≡CH]$^+$ (1) in Dichloromethane under the TD-DFT Calculations

			contribution (%)			Pt components (%)	
orbital	energy (eV)	bond type	Pt	trpy	C≡C		
$37a_1$	−1.3293	d(Pt) + π*(trpy)	39.4	48.7	9.7		31.5 $d_{x^2-y^2}$
$7a_2$	−1.9824	π*(trpy)		97.6			
$10b_1$	−2.0210	π*(trpy)		99.6			
$6a_2$	−2.9040	π*(trpy)		98.4			
$9b_1$	−3.3789	π*(trpy)		93.8			
		HOMO−LUMO Energy Gap					
$8b_1$	−6.8244	d(Pt) + π(C≡C)	47.2	11.3	41.7		46.9 d_{yz}
$27b_2$	−7.0965	d(Pt) + π(C≡C)	29.5	17.1	52.8		29.0 d_{xy}
$36a_1$	−7.2255	d(Pt)	94.9			14 s	80.7 d_{z^2}
$5a_2$	−7.4723	d(Pt) + π(trpy)	63.9	36.0			63.9 d_{yz}
$4a_2$	−7.9376	d(Pt) + π(trpy)	16.0	84.0			16.0 d_{xz}
$7b_1$	−8.4410	d(Pt) + π(trpy) + π(C≡C)	20.8	54.9	24.4		20.5 d_{yz}
$6b_1$	−8.7469	d(Pt) + π(trpy) + π(C≡C)	19.5	70.4	8.3		19.4 d_{xz}

same symmetry and transition character for each complex, the phosphorescent emissions should come from the lowest-energy absorptions. The Stokes shifts between the lowest-energy absorptions and emissions are 0.25 (**1**), 0.22 (**2**), and 0.10 eV (**3**), respectively. The modest shifts are in agreement with the little change between the ground- and excited-state structures.

The 513 nm emission of **1** is assigned to the phosphorescent emission arising from $^3A_1 \rightarrow {}^1A_1$ transition. Table 7 shows the partial molecular orbital compositions of **1** for further understanding the emissive state. As seen from Table 7, the unoccupied MOs ranging from LUMO to LUMO+3 are significantly localized on the terpyridyl ligand above 90% compositions, whereas the LUMO+4 ($37a_1$) involves about 40% metal Pt(II) components. The analogous trend has been observed from the absorption spectrum for **1**. All occupied MOs can be assigned as the participation of Pt(II) atomic orbital. The $8b_1$ (HOMO) and $27b_2$ MOs are composed of metal Pt(II), acetylide, and some terpyridyl ligands. The former is comprised of ca. 47% d_{yz} (Pt), 42% π-bonding (C≡C), and 11% π-conjugation (tryp) and the latter is mainly contributed from ca. 29% d_{xy} atomic orbital (Pt(II)), 53% π-bonding (C≡C), and 17% π-conjugation (trpy), respectively. The $36a_1$ and $37a_1$ MOs have the largest metal compositions in occupied and unoccupied orbitals, respectively. The $36a_1$ MO, lying at −7.2 eV, can be characterized as 95% metal Pt(II) ($5d_{z^2}$ + 6s), whereas $37a_1$ MO, higher than $36a_1$ about 5.9 eV, contains ca. Pt(II) 32% $d_{x^2-y^2}$ atomic orbital. Because such a large separated energy (5.9 eV) is so much larger than the ^{3}LLCT/^{3}MLCT excitation energy (3.4 eV) that phosphorescence with ^{3}d−d character for **1** is not available. It has been suggested that the deactivation in thermally activated decay is feasible via ^{3}d−d excited states.[8a] According to above analysis, the 513 nm phosphorescence is attributed to the ^{3}LLCT (C≡C ← trpy*) and ^{3}MLCT ($5d_{yz}$ ← trpy*) mixed characters. The electron density diagram for **1** is shown in Figure

TABLE 8: Partial Molecular Orbital Contributions (%) in the Lowest-Energy $^3A_1$ Excited-States for [Pt(trpy)C≡CH$_2$OH]$^+$ (2) in Dichloromethane under the TD-DFT Calculations

			contribution (%)				Pt components (%)	
orbital	energy (eV)	bond type	Pt	trpy	C≡C	CH$_2$OH		
54a′	−2.2730	d(Pt) + π*(trpy)	39.3	54.0	6.4			32.2 $d_{x^2-y^2}$
53a′	−2.3609	π*(trpy)		99.3				
36a″	−2.9895	π*(trpy)		97.5				
52a′	−3.0365	π*(trpy)		99.6				
35a″	−3.9642	π*(trpy)		98.5				
51a′	−4.3939	π*(trpy)		92.7				
		HOMO−LUMO Energy Gap						
34a″	−7.2603	d(Pt) + π(C≡C) + σ(CH$_2$OH)	13.8	11.8	36.4	37.9		12.5 d_{xy}
50a′	−7.4206	d(Pt) + π(C≡C) + σ(CH$_2$OH)	31.5	8.3	50.2	9.5		31.4 d_{yz}
33a″	−8.0193	π(C≡C) + σ(CH$_2$OH)	9.4	7.0	20.1	63.5		8.7 d_{xy}
49a′	−8.2794	d(Pt)	94.9				12.5 s	82.4 d_{z^2}
32a″	−8.4685	d(Pt) + π(trpy)	67.3	32.7				67.3 d_{xz}
31a″	−8.9760	d(Pt) + π(trpy)	12.1	87.9				12.1 d_{xz}
48a′	−9.1434	d(Pt) + π(trpy) + σ(CH$_2$OH)	42.3	26.4	13.7	17.5		42.1 d_{yz}

TABLE 9: Partial Molecular Orbital Contributions (%) in the Lowest-Energy $^3A_1$ Excited-States for [Pt(trpy)C≡CC$_6$H$_5$]$^+$ (3) in Dichloromethane under the TD-DFT Calculations

			contribution (%)				Pt components (%)	
orbital	energy (eV)	bond type	Pt	trpy	C≡C	C$_6$H$_5$		
47a$_1$	−1.3511	d(Pt) + π*(trpy)	40.3	53.5	5.7			32.5 $d_{x^2-y^2}$
8a$_2$	−1.9854	π*(trpy)		97.6				
12b$_1$	−2.0186	π*(trpy)		99.6				
7a$_2$	−2.9089	π*(trpy)		98.4				
11b$_1$	−3.3862	π*(trpy)		92.3				
		HOMO−LUMO Energy Gap						
10b$_1$	−6.1634	d(Pt) + π(C≡C) + π(C$_6$H$_5$)	20.7	5.9	34.8	38.6		20.2 d_{yz}
34b$_2$	−6.9939	d(Pt) + π(trpy) + π(C$_6$H$_5$)	25.0	18.1	46.1	10.5		23.7 d_{xy}
46a$_1$	−7.2358	d(Pt)	94.9				14.3 s	80.6 d_{z^2}
6a$_2$	−7.2500	π(C$_6$H$_5$)				100.0		
5a$_2$	−7.4786	d(Pt) + π(trpy)	63.0	37.0				63.0 d_{xz}
9b$_1$	−7.7670	d(Pt) + π(trpy) + π(C$_6$H$_5$)	47.2	17.4		31.8		47.2 d_{yz}
4a$_2$	−7.9379	d(Pt) + π(trpy)	17.1	82.9				17.1 d_{xz}

5. With the aid of the diagram, we can intuitively understand the emissive process from the $^3A_1 \rightarrow {}^1A_1$ transition. As illustrated in the figure, the $9b_1 \rightarrow 8b_1$ excitation corresponds to the largest CI coefficient of 0.70. The electrons in $9b_1$ (LUMO) are located on the terpyridine but transfers to the Pt(II) atom and acetylide ligand in $8b_1$ MO (HOMO). In addition, the $9b_1 \rightarrow 7b_1$ excitation, corresponding to the CI coefficient of 0.17, and $6a_2 \rightarrow 4a_2$ excitation, corresponding to the CI coefficients of −0.13, involve not only ^{3}MLCT character but some $\pi \rightarrow \pi^*$ contribution. However, in the presence of some interferential excitations, the assignment of 513 nm phosphorescent emission should be in line with the excitation with the largest CI coefficient.

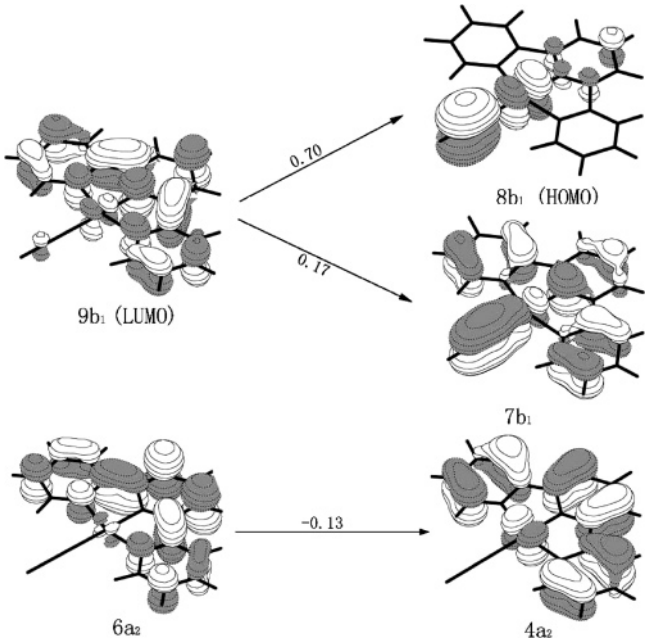

Figure 5. Single electron transition with |CI coefficients| > 0.1 under TD-DFT calculation for the 513 nm emission of [Pt(trpy)C≡CH]$^+$ (**1**) in dichloromethane.

Similar to the listing for **1**, the partial frontier orbital compositions of **2** and **3** are listed in Tables 8 and 9, respectively. As depicted in the tables, the unoccupied MOs of **2** and **3** are still localized on the terpyridine. However, the introduction of CH$_2$OH and C$_6$H$_5$ groups into the acetylide ligand results in difference in compositions of occupied orbitals on going from **1** to **2** and **3**. In particular, in HOMO and HOMO-1, except for the contributions from metal Pt(II) and acetylide ligand, the CH$_2$OH and C$_6$H$_5$ groups are mixed into the HOMO and HOMO-1 and the participation of Pt(II) is decreased sharply in **2** and **3** compared with that in **1**. Therefore, the 584 nm phosphorescence for **2**, arising from the $^3A' \rightarrow {}^1A'$ transition, and 614 nm phosphorescence for **3**, originating from the $^3A_1 \rightarrow {}^1A_1$ transition, are attributed to trpy → Pt/C≡CR (R = CH$_2$OH, C$_6$H$_5$) charge transfer (^{3}LLCT/^{3}MLCT) transition essentially. Yang et al. have detected the lowest-energy 630 nm phosphorescence of [Pt(trpy)C≡CC$_6$H$_5$]$^+$ in the CH$_2$Cl$_2$ solution at room-temperature. Additionally Yam et al. obtained the lowest-energy 552 nm phosphorescence of [Pt(trpy)C≡CCH$_2$OH]$^+$ in the CH$_2$Cl$_2$ solution at room-temperature. They considered that ^{3}MLCT/^{3}LLCT transition is responsible for the

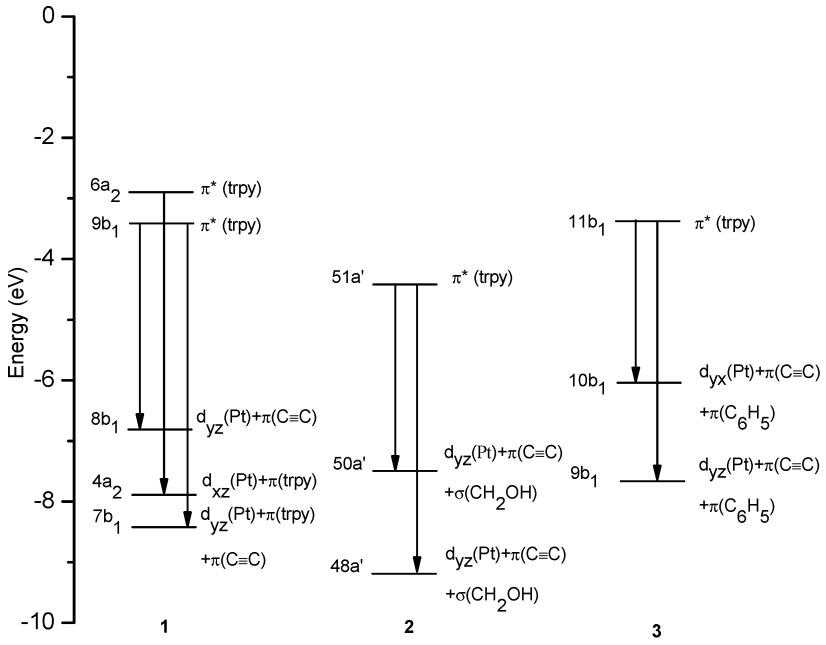

Figure 6. Diagrams of energy levels of orbitals involved in the phosphorescent emissions for $[Pt(trpy)C{\equiv}CH]^+$ (**1**), $[Pt(trpy)C{\equiv}CCH_2OH]^+$ (**2**), and $[Pt(trpy)C{\equiv}CC_6H_5]^+$ (**3**) under TD-DFT calculations.

lowest energy phosphorescence for the two complexes whatever solutions are used.

The electron density diagrams of emissions for **2** and **3** are illustrated in Figure S3 and S4 to help us rationalizing the transitions better. Diagrams of orbital energy levels of **1**−**3** are depicted in Figure 6 to describe the substituent effects on phosphorescent emission. The diagrams list the excited states corresponding to CI coefficient > 0.1 in the configuration wave function. As expected from the diagrams, HOMO−LUMO energy gaps for **1**−**3** decrease in the order 3.45 (**1**) > 2.87 (**2**) > 2.78 (**3**) eV, which are consistent with the ability of electron-donating of the group C_6H_5 > CH_2OH > H. Moreover, the introduction of substituents causes a red shift of phosphorescent emission on going from **1**−**3**. From the above analysis, it can be anticipated when the electron-donating ability of ligand on acetylide is stronger than that of C_6H_5 group, the excitation energy related to emission will be decreased further.

IV. Conclusions

The MP2 and CIS methods are carried out to optimize the ground- and excited-state structures of **1**−**3**. On the basis of their optimized structures, the absorption and emission spectra in the CH_2Cl_2 solution are obtained by the TD-DFT method associated with the PCM model, respectively. Taking into account the variation of substituents on acetylide ligand, the following conclusions can be drawn.

Complexes **1**−**3** have similar structures in both the ground and excited states with the variation of the substituents on acetylide ligand. The minor change of structures between the ground and excited states results in the little stokes shift between the lowest-energy absorption and emission for **1**−**3**.

The lowest-energy absorptions are attributed to the LLCT/MLCT transitions, whereas the lowest-energy emissions are assigned as a ^{3}LLCT/^{3}MLCT origin. When the electron-donating substituents are introduced into the acetylide ligand, the lowest-lying absorption and emission are red-shifted in the order **1** < **2** < **3**.

The absorption spectra in dichloromethane for **1**−**3** are simulated with the Gaussian curves, in which the maxima of the first two lowest-energy absorptions are red-shifted as the ability of electron-donating groups increases; however, those of other absorption bands only slightly change.

In the competition of d−d and charger transfer transitions, the energy gaps between the d−d and charger transfer are separated largely as the introduction of electron-donating substituents into acetylide ligand.

By comparison of the results obtained by using different functionals in TD-DFT method, the calculations indicate that the exchange-correlation functionals (B3LYP, B3P86, and B3PW91) involving Becke three parameter hybrid functionals are appropriate for the terpyridyl Pt(II) acetylide complexes to get the relatively satisfactory results for the absorption spectra. The underestimated excitation energies of lowest-lying absorption bands are probably due to insufficient flexibility in TD-DFT method to describe states with large charge transfer. A similar conclusion has been presented by Roos and co-workers.[20]

Acknowledgment. This work is supported by the Natural Science Foundation of China (20173021, 20333050).

Supporting Information Available: Table S1, showing a comparison of the calculated excitation energies of the absorption bands with LLCT/MLCT and MLCT characters, respectively, by using different functionals in TD-DFT method, Figures S1−S4, showing the density diagrams of the single electron transition both in absorption and emission for **2** and **3**, and tables showing forty vertical transitions with excitation energy and oscillator strength in absorption for **1**−**3**. This material is available free of charge via the Internet at http://pubs.acs.org.

References and Notes

(1) (a) Yersin, H. *J. Chem. Phys.* **1978**, *68*, 4707. (b) van Slageren, J.; Klein, A.; Záliхf0, S. *Coord. Chem. Rev.* **2002**, *230*, 193. (c) Klein, A.; van Slageren, J.; Záliхf0, S. *J. Organomet. Chem.* **2001**, *620*, 202. (d) Klein, A.; van Slageren, J.; Záliхf0, S. *Eur. J. Inorg. Chem.* **2003**, 1927. (e) Benito, J.; Berenguer. J. R.; Forniés, J.; Gil, B.; Gómez, J.; Lalinde, E. *Dalton Trans.* **2003**, 4331. (f) Emmert, L. A.; Choi, W.; Marshall, J. A.; Yang, J.; Meyer, L. A.; Brozik, J. A. *J. Phys.* Chem. A. **2003**, *107*, 11340. (g) Schindler, J. W.; Fukuda, R. C.; Adamson, A. W. *J. Am. Chem. Soc.* **1982**, *104*, 3596.

(2) (a) Lu, W.; Michael, C. W. C.; Cheung, K. K.; Che, C. M. *Organometallics* **2001**, *20*, 2477 (b) Baralt, E.; Boudreaux, E. A.; Demas, J. N.; Lenhert, P, G.; Lukehart, C. M.; Mcphail, A. T.; McPhail, D. R.; Myers, J. B., Jr., Sacksteder, L.; Truela, W. R. *Organometallics* **1989**, *8*, 2417. (c) Sonogashira, K.; Takahashi, S.; Hagihara, N. *Macromolecules* **1977**, *10*, 879. (d) Lechner, A.; Gliemann, G. *J. Am. Chem. Soc.* **1989**, *111*, 7469. (e) Preston, D. M.; Giintner, W.; Lechner, A.; Gliemann, G.; Zink, J. I. *J. Am. Chem. Soc.* **1988**, *110*, 5628. (f) Rice, S. F.; Gray, H. B. *J. Am. Chem. Soc*. **1983**, *105*, 4571. (g) Che, C. M.; Butler, L. G.; Gray, H. B. *J. Am. Chem. Soc.* **1981**, *10*, 3, 7796.

(3) (a) Miskowski, V. M.; Houlding, V. H. *Inorg. Chem.* **1991**, *30*, 4446. (b) Miskowski, V. M.; Houlding, V. H. *Inorg. Chem.* **1989**, *28*, 1529. (c) Bailey, J. A.; Hill, M. G.; Marsh, R. E.; Miskowski, V. M.,; Schaefer, W. P.; Gray, H. B. *Inorg. Chem.* **1995**, *34*, 4591. (d) Isci, H.; Mason, W. R. *Inorg. Chem.* **1975**, *14*, 905. (e) Houlding, V. H.; Miskowski, V. M. *Coord. Chem. Rev.* **1991**, *91*, 145. (f) Lai, S. W.; Chan, M. C. W.; Cheung, K. K.; Che, C. M. *Organometallics* **1999**, *18*, 3327. (g) Yip, J. H. K.; Vittal, J. J. *Inorg. Chem.* **2000**, *39*, 3537. (h) Yang, Q. Z.; Wu, L. Z.; Zhang, H.; Chen, B.; Wu, Z. X.; Zhang. L. P.; Tung, C. H. *Inorg. Chem.* **2004**, *43*, 5195. (i) Lu. W.; Mi, B. X.; Chan, C. W.; Hui, Z.; Che, C. M.; Zhu, N. Y.; Lee, S. T. *J. Am. Chem. Soc.* **2004**, *126*, 4958. (j) Willison, S. A.; Jude, H.; Antonelli, R. M.; Rennekamp, J. M.; Eckert, N. A.; Bauer, J. A. K.; Connick, W. B. *Inorg. Chem.* **2004**, *43*, 2548. (k) Miskowski, V. M.; Houlding, V. H. *Inorg. Chem.* **1989**, *28*, 1529. (l) Bailey, J. A.; Miskowski, V. M.; Gray, H. B. *Inorg. Chem.* **1993**, *32*, 369. (m) Miskowski, V. M.; Houlding, V. H.; Che, C. M.; Wang Yu. *Inorg. Chem.* **1993**, *32*, 2518.

(4) (a) Yam, V. W. W.; Tang, R. P. L.; Wong, K. M. C.; Cheung, K. K. *Organometallics* **2001**, *20*, 4476. (b) Yang, Q. Z.; Wu, L. Z.; Wu, Z. X.; Zhang, L. P.; Tung, C. H. *Inorg. Chem.* **2002**, *41*, 5653. (c) Guo, F. Q.; Sun, W. F.; Liu, Y.; Schanze, K. **2005**, *44*, 4055.

(5) Aldridge, T. K.; Elizabeth, M. S.; McMillin, D. R. *Inorg. Chem.* **1994**, *33*, 722.

(6) (a) Michalec, J. F.; Bejune, S. A.; Cuttell, D. G.; Summerton, G. C.; Gertenbach, J. A.; John, S. F.; Raymond, J. H.; McMillin, D. R. *Inorg. Chem.* **2001**, *40*, 2193. (b) Büchner, R.; Cunningham, C. T.; Field, J. S.; Haines, R. J.; McMillin, D. R.; Summerton, G. C. *J. Chem. Soc., Dalton Trans.* **1999**, 711. (c) Michalec, J. F.; Bejune, S. A.; McMillin, D. R. *Inorg. Chem.* **2000**, *39*, 2708. (d) Crites, D. K.; Cunningham, C. T.; McMillin, D. R. *Inorg. Chem. Acta.* **1998**, *273*, 346.

(7) Lai, S. W.; Chan, M. C. W.; Cheung, K. K.; Che, C. M. *Inorg. Chem.* **1999**, *38*, 4262.

(8) Yip, H. K.; Cheng, L. K.; Cheung, K. K.; Che, C. M. *J. Chem. Soc., Dalton Trans.* **1993**, 2993.

(9) Büchner, R.; Field, J. S.; Haines, R. J.; Cunningham, C. T.; McMillin, D. R. *Inorg. Chem.* **1997**, *36*, 3952.

(10) Bailey, J. A.; Hill, M. G.; Marsh, R. E.; Miskowski, V. M.; Schaefer, W. P. Gray, H. B. *Inorg. Chem.* **1995**, *34*, 4591.

(11) (a) Frisch, M. J.; Head-Gordon. M.; Pople, J. A. *Chem. Phys. Lett.* **1990**, *166*, 275. (b) Frisch, M. J.; Head-Gordon, M.; Pople, J. A. *Chem. Phys. Lett.* **1990**, *166*, 281. (c) Head-Gorden, M.; Pople, J. A.; Frisch, M. J. *Chem. Phys. Lett*. **1988**, *153*, 503. (d) Head-Gorden, M.; Head-Gorden, T. *Chem. Phys. Lett.* **1994**, *220*, 122.

(12) (a) Stanton, J. F.; Gauss, J.; Ishikawa, N.; Head-Gordon, M. *J. Chem. Phys.* **1995**, *103*, 4160. (b) Foreman, J. B.; Head-Gordon, M.; Pople, A. *J. Phys. Chem.* **1992**, *96*, 135. (c) Waiters, V. A.; Hadad, C. M.; Thiel, Y.; Colson, S. D.; Wibergy, K. B.; Johnson, P. M.; Foresmanl, J. B. *J. Am. Chem. Soc.* **1991**, *113*, 4782.

(13) (a) Casida, M. E.; Jamorski, C.; Casida, K. C.; Salahub, D. R. *J. Chem. Phys.* **1998**, *108*, 4439. (b) Stratmann, R. E.; Scuseria, G. E. *J. Chem. Phys.* **1998**, *109*, 8218. (c) Matsuzawa, N. N.; Ishitani, A. *J. Phys. Chem. A.* **2001**, *105*, 4953.

(14) Becke, A. D. *J. Chem. Phys.* **1993**, *98*, 5648.

(15) (a) Cossi, M.; Scalmani, G.; Regar, N.; Barone, V. *J. Chem. Phys.* **2002**, *117*, 43. (b) Barone, V.; Cossi, M. *J. Chem. Phys*. **1997**, *107*, 3210.

(16) (a) Bauernschmitt, R.; Ahlrichs, R. *Chem. Phys. Lett.* **1996**, *256*, 454. (b) Farrell, I. R.; van Slageren, J.; Zâli×f0, S.; Vlèek, A., Jr. *Inorg. Chem. Acta.* **2001**, *315*, 44. (c) Rosa, A.; Baerends, E. J.; van Gisbergen, S. J. A. V.; van Lenthe, E.; Groeneveld, J. A.; Snijders, J. G. *J. Am. Chem. Soc.* **1999**, *121*, 10356.

(17) (a) Wadt, W. R.; Hay, P. J. *J. Chem. Phys.* **1985**, *82*, 284. (b) Hay, P. J.; Wadt, W. R. *J. Chem. Phys.* **1985**, *82*, 299.

(18) Dolg, M.; Pyykkö, P.; Runeberg, N. *Inorg. Chem.* **1996**, *35*, 7450.

(19) Frisch, M. J.; Trucks, G. W.; Schlegel, H. B.; Scuseria, G. E.; Robb, M. A.; Cheeseman, J. R.; Montgomery, J. A., Jr.; Vreven, T.; Kudin, K. N.; Burant, J. C.; Millam, J. M.; Iyengar, S. S.; Tomasi, J.; Barone, V.; Mennucci, B.; Cossi, M.; Scalmani, G.; Rega, N.; Petersson, G. A.; Nakatsuji, H.; Hada, M.; Ehara, M.; Toyota, K.; Fukuda, R.; Hasegawa, J.; Ishida, M.; Nakajima, T.; Honda, Y.; Kitao, O.; Nakai, H.; Klene, M.; Li, X.; Knox, J. E.; Hratchian, H. P.; Cross, J. B.; Bakken, V.; Adamo, C.; Jaramillo, J.; Gomperts, R.; Stratmann, R. E.; Yazyev, O.; Austin, A. J.; Cammi, R.; Pomelli, C.; Ochterski, J. W.; Ayala, P. Y.; Morokuma, K.; Voth, G. A.; Salvador, P.; Dannenberg, J. J.; Zakrzewski, V. G.; Dapprich, S.; Daniels, A. D.; Strain, M. C.; Farkas, O.; Malick, D. K.; Rabuck, A. D.; Raghavachari, K.; Foresman, J. B.; Ortiz, J. V.; Cui, Q.; Baboul, A. G.; Clifford, S.; Cioslowski, J.; Stefanov, B. B.; Liu, G.; Liashenko, A.; Piskorz, P.; Komaromi, I.; Martin, R. L.; Fox, D. J.; Keith, T.; Al-Laham, M. A.; Peng, C. Y.; Nanayakkara, A.; Challacombe, M.; Gill, P. M. W.; Johnson, B.; Chen, W.; Wong, M. W.; Gonzalez, C.; Pople, J. A. *Gaussian 03*, revision C.02. Gaussian, Inc.: Wallingford, CT, 2004.

(20) Tozer, D. J.; Amos, R. D.; Handy, N. C.; Roos, B. O.; Serrano-Andres, L. *Mol. Phys.*. **1999**, *97*, 859.